ROYAL SOCIETY
OF CHEMISTRY

Check for updates

Mechanistic elucidation of irreversible chemodosimetric sensing of hydrazine through structural, computational, and bioimaging analyses

Priyanka Avala,[ab] Malavika S Kumar,[ab] Avijit Kumar Das, [ID] *[ab] Ankan Sardar,[c] Tilak Raj Maity,[d] Aveek Samanta[e] and Malay Dolai [ID] *[f]

A fluorescent chemodosimeter, **DBA**, has been developed for the selective detection of hydrazine *via* an irreversible reaction pathway that leads to fluorescence enhancement. The crystal structure of the ligand has been successfully determined. The sensing mechanism involves the conversion of a hydrazide derivative into a hydrazone derivative, as confirmed by both ^{1}H NMR and mass spectrometry. Upon interaction of **DBA** with hydrazine, the probe exhibits a significant decrease in absorbance at 366 nm and 279 nm, along with a three fold enhancement in fluorescence intensity at 423 nm, achieving a detection limit of 0.37 μM. The detection mechanism has also been supported by theoretical analysis using density functional theory (DFT) calculations. For practical applications, **DBA** has been employed in plant-based cell imaging to monitor hydrazine accumulation in *Lathyrus sativus L.* (grass pea). Overall, **DBA** is a simple, effective, and promising fluorescent probe for hydrazine detection in diverse fields such as environmental monitoring, food safety, and biological risk assessment.

1. Introduction

Fluorescent chemosensors are compounds that integrate a fluorescent unit (fluorophore), a specific binding site for the target analyte, and a mechanism that involves the interaction between these two components. The indicators are referred to as fluorescent chemodosimeters if the binding sites have irreversible chemical processes.[1–6] The concept of chemodosimeters was first introduced by Chae and Czarnik in 1992.[7–9] In chemodosimetric sensing, the presence of the target analyte triggers both the breaking and forming of chemical bonds, resulting in products structurally distinct from the original sensor. The creation of chemodosimeters for both the identification and quantification of various substances is a relatively recent

development in scientific research. Techniques based on colour changes (colorimetric) and fluorescence (fluorometric) are widely used because they are affordable, highly selective, sensitive, and efficient and provide rapid results for detecting different analytes.[10–14] In particular, colorimetric and fluorescence-based sensors that allow naked-eye detection have gained significant attention for their simplicity, rapid operation, and capability for real-time analysis. Chemosensors are now widely employed for monitoring hazardous substances and environmental contaminants in a variety of samples, because of their outstanding sensitivity, broad detection range, adaptable design, and strong resistance to interference.[15–18]

Hydrazine (N_2H_4), a colourless, fuming liquid with strong reducing properties, is a highly reactive compound crucial to industrial and technological applications. It is a highly energetic compound, a hexatomic molecule comprising two nitrogen atoms and four highly reactive hydrogen atoms, which easily reacts with oxygen and other elements during chemical combustion or transformation. Globally, its production reached around 200 000 metric tons annually a decade ago, driven by its versatile uses.[19] Hydrazine and its derivatives remain key fuels in bipropellant rocket engines due to their ability to release substantial energy through exothermic reactions.[20] It serves as an effective fungicide and is also used in the synthesis of pesticides like maleic hydrazide, manufacturing plastic foams, and controlling grass growth in residential areas.[21] Hydrazine derivatives treat

[a] *Department of Chemistry, Christ University, Hosur Road, Bangalore, Karnataka 560029, India. E-mail: avijitkumar.das@christuniversity.in, sanjuavi.das@gmail.com*
[b] *Centre for Renewable Energy and Environmental Sustainability, Christ University, Karnataka, 560029, India*
[c] *Department of Chemical Sciences, Indian Institute of Science Education and Research (IISER) Kolkata, Mohanpur 741246, India*
[d] *Department of Biotechnology, Haldia Institute of Technology, Haldia, Purba Medinipur–721657, West Bengal, India*
[e] *Department of Botany, Prabhat Kumar College, Contai, Purba Medinipur 721404, W.B., India*
[f] *Department of Chemistry, Prabhat Kumar College, Purba Medinipur 721404, West Bengal, India. E-mail: dolaimalay@yahoo.in*

conditions such as hypertension,[22] urinary tract infections,[23] and tuberculosis.[24] It acts as an oxygen scavenger in boiler feedwater to prevent corrosion. Dual-injection of hydrogen and hydrazine into reactor water is regarded as a novel approach to minimize stress corrosion cracking (SCC) in boiling water reactors (BWRs).[25] This compound's adaptability across aerospace, agriculture, medicine, and energy sectors underscores its industrial significance despite handling challenges posed by its reactivity. The U.S. Environmental Protection Agency has established a 10-ppb threshold limit value (TLV) for hydrazine exposure, derived from animal as well as human studies.[26] Therefore, the lower limit of detection of hydrazine is very much important. In this respect, use of fluorescent sensors has emerged as a superior method for detecting hydrazine compared to traditional analytical techniques like liquid chromatography,[27] mass spectrometry,[28,29] potentiometry,[30] and titrimetry.[31] These conventional methods face limitations such as complex buffer preparation, time-consuming protocols, low sensitivity, and destructive sample processing unsuitable for live biological systems.[32] Fluorescent probes address these challenges through enhanced features like straightforward operation, exceptional molecular selectivity, and ultra-low detection limits, reaching submicromolar concentrations.[33]

Recent progress in the development of fluorescent chemosensors for selective hydrazine detection holds considerable importance due to their wide-ranging applications in medical and environmental research.[34–37] In recent years, the development of small-molecule fluorescent probes has accelerated significantly, employing a variety of molecular recognition approaches such as protecting-group removal, nucleophilic substitution, and chemodosimetric reactions that transform non-fluorescent precursors into strongly emissive products. Several recent reviews have comprehensively summarized these strategies and their relevance to environmental and biological hydrazine detection.[38–40] Current trends in probe design focus on achieving ratiometric and near-infrared (NIR) emission responses, which enhance quantitative accuracy in complex systems and support applications in deep-tissue imaging and on-site sensing.[41] Despite these advances, many existing sensors continue to exhibit drawbacks such as limited solubility in aqueous media, cross-reactivity with other nucleophiles, and challenging synthetic routes. Thus, there remains a strong demand for straightforward, highly selective chemodosimeters capable of reliable hydrazine detection in real samples—an objective that the present study seeks to fulfil. Colorimetric and fluorimetric sensors for the naked-eye detection have attracted considerable interest because of their simple and fast implementation as well as their high sensitivity. Herein, we have developed a chemodosimeter by mixing 2,4-di-*tert*-butyl-5,6-catechol-1-aldehyde with acetohydrazide in ethanol medium to produce target ligand **DBA**, which has been characterized by ^{1}H-NMR, ^{13}C-NMR, mass spectroscopy (Fig. S3–S5) and X-ray crystal analysis. Although several reports are available on the selective detection of hydrazine, we have included a comparison table in the SI that summarizes recent studies on related ligands (Table S1). The comparison table indicates that although hydrazine is the common analyte across all reported systems, our probe (**DBA**) achieves a substantially lower LOD than previously reported complexes. A key strength of this study is the structural characterization of the ligand through single-crystal X-ray diffraction, which provided an accurate molecular model for DFT calculations and ensured excellent agreement between experimental and theoretical results. Overall, the comparison highlights the superior performance of **DBA** across multiple parameters, underscoring its strong potential for diverse applications.

2. Results and discussion

2.1. Synthesis and characterization of DBA

The solution of 4,6-di-*tert*-butyl-2,3-dihydroxybenzaldehyde (226 mg, 1 mmol) in methanol and the solution of acetohydrazide (74 mg, 1 mmol) in methanol was mixed together (Scheme 1). Then the mixture was stirred for another 1 hour. A bright yellowish colored solution appeared. It was stirred for 2 hours more to complete the reaction by TLC monitoring. The yellow precipitate of (*E*)-*N*′-(4,6-di-*tert*-butyl-2,3-dihydroxybenzylidene) acetohydrazide (**DBA**) was separated out by filtration and the residue was washed with cold methanol and dried. The block type yellow crystals were obtained after 4 days by slow evaporation of methanol solvent. Mp: 110–120 °C, yield: 200 mg, 72%. ^{1}H NMR (DMSO-d_6, 400 MHz): 12.77 (s, 1H, –OH), 10.67 (s, 1H, –OH), 8.75 (s, 1H), 6.82 (s, 1H), 1.44 (s, 9H), 1.36 (s, 12H). ^{13}C NMR (DMSO-d_6, 100 MHz): 197.4, 152.6, 142.4, 142.3, 141.7, 116.1, 114.7, 35.4, 35.3, 33.3, 28.8. Mass (*m/z*, %): M$^+$ calculated

4,6-di-*tert*-butyl-2,3-dihydroxybenzaldehyde   acetohydrazide

(*E*)-*N*′-(4,6-di-*tert*-butyl-2,3-dihydroxybenzylidene)acetohydrazide (**DBA**)
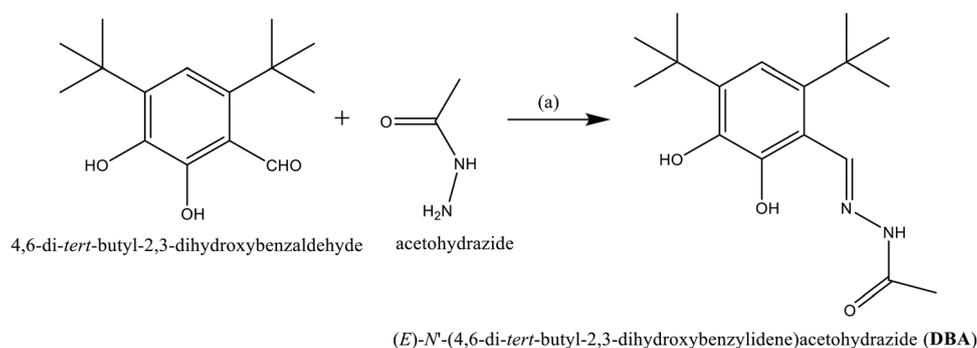
Scheme 1 Synthetic procedure of **DBA**.

for chemical formula: $C_{17}H_{26}N_2O_3$ is 306.4060; found: 307.5123 $(M+H)^+$.

2.2. X-ray crystal analysis of DBA

Several spectroscopic methods are employed to determine the structure and chemical formula of the probe **DBA**. The crystal structure of **DBA** is determined by the single crystal X-ray diffraction (SCXRD) technique (CCDC no. 2472615). The crystal X-ray study indicates that the sensor **DBA** crystallizes in a monoclinic system with the space group $P21/c$. The structure in Fig. 1a shows that the aldehyde and carbohydrazide parts are connected through an imine bond (–C3=N1) with a bond length of 1.276 Å, which is comparable to that of previously reported Schiff base ligands. **DBA** gains stability through the
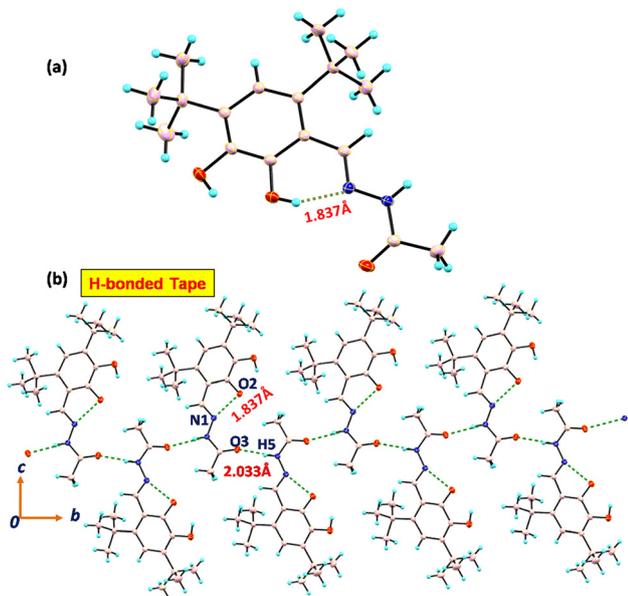

Fig. 1 (a) The ORTEP view (30% ellipsoid probability) of **DBA**; (b) the intermolecular hydrogen bonded (green dashed line) 1D tape along the crystallographic *b* axis; color code: sea green, H; light pink, C; blue, N; and red, O.

formation of intermolecular H-bonding interactions (O3···H5 = 2.033 Å) between adjacent units, allowing them to form a H-bonded 1D tape along the crystallographic *b* axis (Fig. 1b).

2.3. Interference study

The selectivity of **DBA** for N_2H_4 over other interfering analytes like Cl^-, Br^-, I^-, F^-, NO_2^-, AsO_2^{3-}, HSO_4^{2-}, $C_2O_4^-$, H_2O_2, NO_3^-, H_2S, triethylamine (TEA), NH_3, ethylenediamine (EDA), piperidine (Bpy), hypochlorous acid (HClO), and OH^- was evaluated in CH_3CN/HEPES buffer solution (9:1, v/v, pH 7.4). Upon addition of N_2H_4, **DBA** exhibited a distinct increase in emission intensity at 423 nm. In contrast, no significant spectral changes were observed with other anions, confirming the high selectivity of **DBA** towards N_2H_4 (Fig. 2a). In the bar diagram, the brown bar with the highest intensity indicates the fluorescence response of **DBA** toward N_2H_4, while the green bars represent the negligible interference of **DBA** with other analytes (Fig. 2b).

2.4. Spectroscopic response of DBA toward N_2H_4

The interaction between **DBA** and N_2H_4 was examined *via* spectrophotometric titration in CH_3CN/HEPES buffer solution (9:1, v/v, pH 7.4). The ligand **DBA** initially exhibited strong absorption signals at wavelengths 366 nm and 279 nm, which were progressively decreased upon incremental addition of N_2H_4 (Fig. 3a).

Similarly, the fluorescence sensing property of **DBA** towards N_2H_4 was systematically investigated using a fluorescence spectrophotometer in CH_3CN/HEPES buffer (9:1, v/v, pH 7.4) solution at an excitation wavelength of 315 nm. The fluorescence intensity of **DBA** remains stable even at high proportions of water (Fig. S11); however, hydrazine sensing in water-rich media such as CH_3CN/HEPES buffer (5:5, v/v) is challenging. This difficulty arises from the small size, high polarity, and strong hydration of hydrazine, which hinder effective interactions with sensing probes like **DBA**. Moreover, extensive solvation and hydrogen bonding around N_2H_4 further reduce its binding availability, resulting in lower sensitivity and selectivity
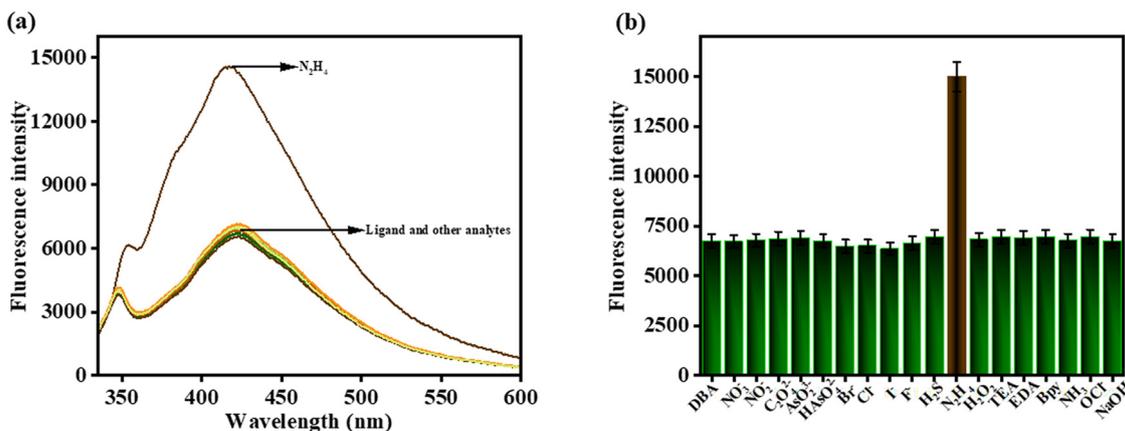
Fig. 2 (a) Comparison fluorescence spectra of **DBA** ($c = 5.0 \times 10^{-5}$ M) upon addition of different guest anions (15 equiv.) in CH_3CN/HEPES buffer solution (9:1, v/v, pH 7.4) (λ_{ex} = 315 nm). (b) A comparative fluorescence response of **DBA** by bar representation in the presence of different anions.
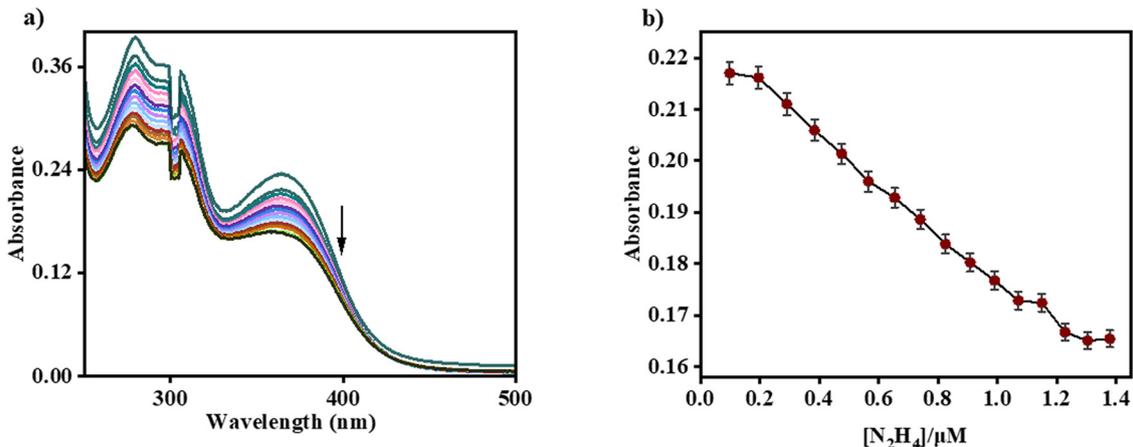
Fig. 3 (a) UV-vis titration spectra of **DBA** ($c = 5.0 \times 10^{-5}$ M) in the presence of N_2H_4 ($c = 1 \times 10^{-5}$ M) in CH_3CN/HEPES buffer solution (9 : 1, v/v, pH 7.4). (b) Absorbance changes of **DBA** vs. N_2H_4 concentration with error bars ranging 1% (Y error bars for both [±] deviation).

(Fig. S12). Fluorescence studies across pH 2–14 reveal that **DBA** exhibits minimal emission at extreme pH values under both strong acidic and basic conditions but strong hydrazine-induced fluorescence near physiological pH, demonstrating optimal sensing performance under biologically relevant conditions (Fig. S9). Initially, **DBA** exhibited two emission signals centered at 350 nm with lower intensity and at 423 nm with high intensity, having a fluorescence quantum yield of $\Phi = 0.0735$. Upon incremental addition of N_2H_4, three fold enhancement in fluorescence intensity was observed with a high fluorescence quantum yield ($\Phi = 0.21$), accompanied by a hypsochromic shift ($\Delta\lambda = 5$ nm) of the emission signal at 418 nm up to a saturation level (Fig. 4a).

The detection limit of **DBA** toward N_2H_4 was evaluated at 0.37 μM through fluorometric analysis utilizing the established relationship $DL = K \times Sb_1/S$, where $K = 3$, Sb_1 represents the standard deviation of blank measurements, and S denotes the calibration curve slope (Fig. S1). Based on the variations in **DBA** fluorescence intensity upon the addition of N_2H_4 at different

time intervals, the rate constant was calculated as 2.705 s^{-1}, using a first-order rate equation, indicating the rapid response of **DBA** toward N_2H_4 (Fig. S2).

2.5. Competition experiment

The competitive sensing ability of **DBA** toward N_2H_4 was evaluated in the presence of various interfering anions in a CH_3CN/HEPES buffer solution (9 : 1, v/v, pH 7.4). The fluorescence enhancement observed upon N_2H_4 binding remained unaffected by the presence of other competing analytes, demonstrating the high sensitivity and selectivity of **DBA** for N_2H_4 even in complex analyte environments (Fig. 5).

2.6. Probable N_2H_4 sensing mechanism in the presence of DBA

The probable sensing mechanism behind the improved fluorescence emission of the ligand **DBA** in the presence of N_2H_4 involves the transformation of the hydrazide derivative (**DBA**) into a hydrazone derivative (**DBH**) (Scheme 2 and Scheme S1).[42] Although **DBA** contains electron-donating hydroxyl groups at
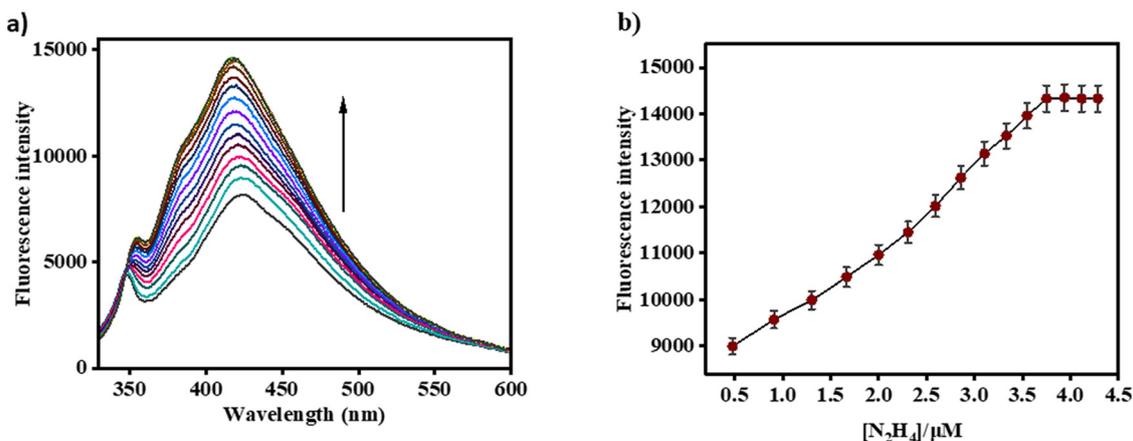

Fig. 4 (a) Fluorescence titration spectra of **DBA** ($c = 5.0 \times 10^{-5}$ M) in the presence of N_2H_4 ($c = 1.0 \times 10^{-5}$ M) in CH_3CN/HEPES buffer solution (9 : 1, v/v, pH 7.4) ($\lambda_{ex} = 315$ nm). (b) Changes in emission intensity as a function of N_2H_4 concentration with error bars ranging 2% (Y error bars for both [±] deviation).
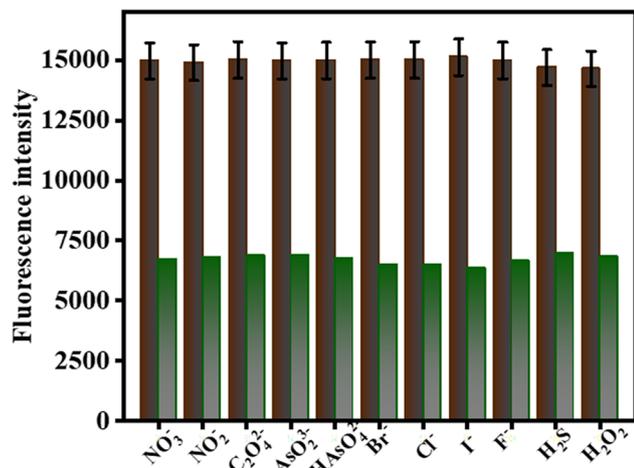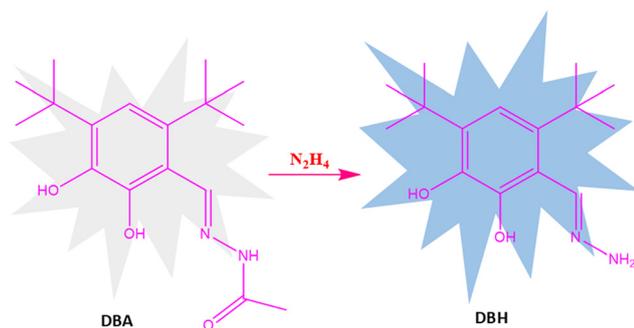
Fig. 5 Fluorescence intensity variation (green bars) of DBA + 15 equiv. of various interfering analytes (A^{n-}); (maroon bars) fluorescence intensity of DBA + 15 equiv. A^{n-}, followed by 10 equiv. of N_2H_4 in CH_3CN/HEPES buffer solution (9 : 1, v/v, pH 7.4) (λ_{ex} = 315 nm).

Scheme 2 Plausible reaction mechanism between **DBA** and N_2H_4.

the *ortho* positions, which promote intramolecular charge transfer (ICT) by increasing electron density across the aromatic system, the presence of the hydrazide group hinders efficient ICT, thereby reducing fluorescence. Moreover, in the solvatochromic analysis, **DBA** exhibited negligible fluorescence enhancement/shifting in most of the tested solvents, namely CH_3CN, CH_3OH, acetone, DMSO, H_2O, toluene, and THF. Notably, weak fluorescence was detected in toluene, with comparatively lower intensities in DMSO and THF, showing two distinct emission bands at 350 nm and 423 nm (Fig. S10). Upon reaction with hydrazine, the ligand **DBA** has been converted to a hydrazone derivative **DBH** featuring an extended conjugated system comprising the aromatic ring, the hydrazone linkage (–C=N–NH$_2$), and two electron-donating hydroxyl groups. This transformation significantly improves ICT within the aromatic ring, which results in an increase in fluorescence upon reacting with N_2H_4.[43] Moreover, the bulky *tert*-butyl groups at the 4 and 6 positions additionally suppress non-radiative decay pathways by restricting rotational and vibrational motions, stabilizing the excited state and resulting in enhanced fluorescence.

Moreover, the conversion of **DBA** to **DBH** was also confirmed through ^{1}H-NMR and mass spectra (Fig. S6 and S7). Upon transformation of the hydrazide group in **DBA** to a hydrazone group in **DBH**, significant shifts in the proton signals were observed, particularly for the two hydroxyl protons attached to the benzene ring and the imine proton. In **DBA**, the hydroxyl proton signals appeared at 12.78 ppm (Ha) and 10.68 ppm (Hb), attributed to strong deshielding effects from the adjacent hydrazide group. In **DBH**, these signals shifted downfield to 12.63 ppm (Ha) and 9.49 ppm (Hb), consistent with the replacement of the hydrazide group by a hydrazone moiety. Additionally, the imine and aromatic protons also showed slight shifts: from 8.77 ppm (Hc) and 6.83 ppm (Hd) in **DBA** to 8.46 ppm (Hc) and 6.85 ppm (Hd) in **DBH** (Fig. S6). The transformation of **DBA** into **DBH** was additionally confirmed by the emergence of a distinctive molecular ion peak at m/z. = 265.4202 $(M + H)^+$, which is close to the theoretical mass peak for $C_{15}H_{24}N_2O_2$ at 264.3690 for **DBH** (Fig. S7).

2.7 Theoretical calculation

To elucidate the sensing mechanism of **DBA** toward N_2H_4 through the formation of **DBH**, structural optimizations were carried out using density functional theory (DFT) at the B3LYP level (Fig. 6a). Additionally, we examined the spatial electron cloud distribution and calculated the frontier molecular orbital energies—specifically the highest occupied molecular orbital
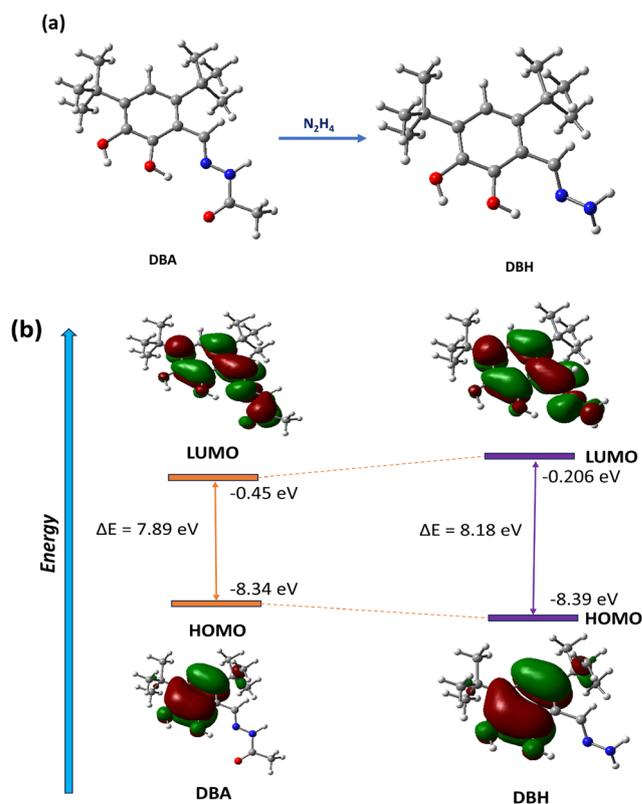

Fig. 6 (a) Geometry optimized molecular structure of (i) **DBA** and (ii) **DBH** (**DBA** + N_2H_4). (b) Frontier molecular orbital with the energy difference of (i) **DBA** and (ii) **DBH** (**DBA** + N_2H_4).

(HOMO) and the lowest unoccupied molecular orbital (LUMO)—for both **DBA** and **DBH**. For **DBA**, the energy gap between the HOMO (-8.34 eV) and LUMO (-0.45 eV) is 7.89 eV. In contrast, **DBH** exhibits a slightly larger HOMO–LUMO energy gap of 8.18 eV, with HOMO and LUMO energies of -8.39 eV and -0.206 eV, respectively (Fig. 6b). Notably, the stabilization of the HOMO level in **DBH** and the observed increase in the HOMO–LUMO energy gap from 7.89 eV (**DBA**) to 8.18 eV (**DBH**) suggest the thermodynamic feasibility of the conversion from **DBA** to **DBH**. The production of **DBH** is indicated by one absorption band at 366 nm in methanolic solution at 25 °C, and the theoretically calculated absorbance is 370 nm, which is well supported by experimental results. This spectrum is caused by the $S_0 \rightarrow S_8$ transitions that occur during **DBH** formation.

2.8. Root imaging study

In this study, we have demonstrated the potential of a fluorescent probe, **DBA**, for detecting hydrazine accumulation using a plant-based cell imaging approach. The legume *Lathyrus sativus* L. (grass pea) was employed as a cost-effective, convenient, and readily available model system for primary screening.[44,45] Transverse sections of treated roots displayed clear fluorescence signals, indicating the successful accumulation and interaction of **DBA** with N_2H_4 (Fig. 7IB and D). Moreover, root extracts subjected to centrifugation and observed under UV light revealed strong blue fluorescence in the **DBA** and hydrazine-treated samples. The higher fluorescent zone is observed inside xylem upon treatment. This signifies that the chemical **DBA** is absorbed by the root and transported with water throughout the plant in contrast to the non-fluorescent control (Fig. 7IA and C). These results validate the efficacy of **DBA** as a reliable indicator of hydrazine presence in plant tissues. We proposed **DBA** as an advanced fluorescent probe in this study, which offers a promising, simple, and effective approach for hydrazine detection across various domains, including environmental monitoring, food safety assessment, and biological risk evaluation.

The antioxidant activity of **DBA** was assessed using the DPPH radical scavenging assay. As shown in Fig. 7(I), the control containing only the DPPH reagent retained a strong purple coloration, suggestive of unreacted DPPH radicals. In contrast, the **DBA** treated samples demonstrated a significant reduction in the intensity of the purple color, signifying the presence of active antioxidant compounds capable of neutralizing free radicals. 50% reduction was seen at 10 μM concentration of **DBA**. The degree of decolorization visually suggested a concentration-dependent effect, where higher sample concentrations of **DBA** led to more pronounced fading. At higher concentrations (30–50 μM), the extent of fading appeared to be similar across treatments, indicating that the scavenging activity reached a plateau. Based on the visual inspection of color intensities, there is a significant difference between the control and all DBA treated samples. However, no significant difference is visually detectable among the 30 μM, 40 μM, and 50 μM treatments, suggesting that DPPH radicals were maximally scavenged at 30 μM and additional increases in concentration did not further enhance activity. Overall, the data indicate that DBA possesses strong antioxidant potential, with significant activity evident from 10 μM onward (Fig. 7II). This color transition from deep purple to lighter hues confirms the radical scavenging ability of **DBA**, underscoring its potential as a source of potential antioxidant compounds.[46] Hydrazine (N_2H_4) is a volatile and highly toxic compound known to cause significant harm to water, soil, air, and living organisms. Numerous earlier studies have reported its carcinogenic potential following toxic or even subtoxic exposure.[47,48] Given its wide industrial use in pharmaceuticals, pesticides, and textile dye production, hydrazine must be detected in real time and monitored in the environment for an extended period of time in order to preserve the environment and the health of humanity. Once absorbed by plants, hydrazine can infiltrate
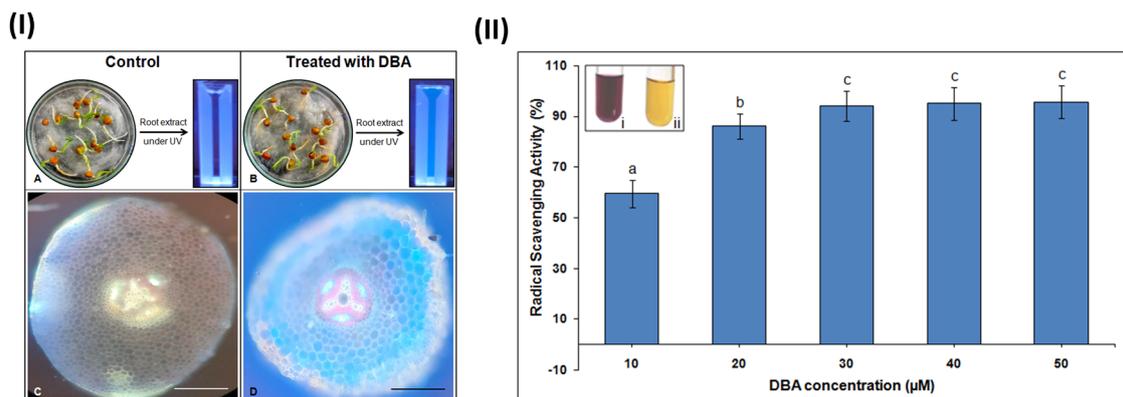

Fig. 7 (I) Estimation of hydrazine (N_2H_4) in grass pea roots. (A) Fluorescence of the root extract under UV light and seedlings treated with distilled water (control). (B) Fluorescence of the root extract under UV light and seedlings treated with N_2H_4 followed by **DBA**. Transverse sections of roots imaged under UV light: (C) control root, (D) treated root (N_2H_4 + **DBA**). Scale bar = 10 μm. (II) Antioxidant activity of **DBA** in the presence of DPPH. In accordance with Duncan's multiple range test, the data indicated by different lower-case letters are significantly distinct ($p \leq 0.05$), and the data are displayed as mean ± standard deviation (n = 10). The inset presents the degree of color fading (purple to yellow) proportional to antioxidant capacity, (i) only 0.1 μM DPPH and (ii) 0.1 μM DPPH + 50 μM **DBA**.

the food chain, exacerbate oxidative stress, induce lipid peroxidation, stimulate reactive oxygen species (ROS) formation, and ultimately damage essential biomolecules such as DNA, proteins, and cellular structures.

2.9. Soil analysis

Chemicals used in warfare are most commonly found in the soil of areas that once served as battlefields, where they have been released into the environment.[49] So, we have performed real-time field soil analysis, to understand the selectivity for hydrazine. 1 g of field soil was placed in separate vials along with the ligand **DBA** ($c = 5.0 \times 10^{-5}$ M), in the presence of hydrazine ($c = 1.0 \times 10^{-5}$ M). In the fluorescence study, as the concentration of hydrazine increased, the corresponding emission intensity progressively increased. And from this titration, the detection limit was calculated and found to be 0.029 μM (Fig S8, SI). These findings confirm that the **DBA** probe is suitable for real-time hydrazine detection in environmental samples, especially soil.

3. Conclusion

In conclusion, the fluorescent chemodosimeter **DBA** offers a highly efficient, selective, and sensitive platform for hydrazine detection *via* an irreversible reaction pathway that produces a pronounced enhancement in fluorescence intensity. The sensing mechanism, based on the transformation of the hydrazide group into its corresponding hydrazone form, is strongly supported by ^{1}H NMR and mass spectrometric analyses and theoretical studies, confirming both structural changes and the mechanistic reliability of the system. **DBA** exhibits excellent photostability, rapid response behavior, and an exceptionally low detection limit, establishing it as a robust probe for diverse analytical applications. Its high biocompatibility and low cytotoxicity further enable effective plant-based cellular imaging, successfully visualizing hydrazine accumulation in *Lathyrus sativus* L. (grass pea). Additionally, **DBA** was used to detect hydrazine in environmental samples through soil analysis experiments, *i.e.*, real environmental analysis. These results establish **DBA** as a promising candidate for biological, environmental, and analytical sensing applications. Future improvements in its molecular design could enhance solubility, spectral properties, and sensing performance, broadening its suitability for *in vivo* imaging. Coupling **DBA**-based probes with portable devices, microfluidic platforms, or nanomaterial interfaces may further expand their use in environmental monitoring, food quality analysis, and biomedical diagnostics. Overall, **DBA** shows strong promise as a versatile fluorescent sensor for advanced analytical and biosensing technologies.

Conflicts of interest

There are no conflicts of interest to declare.

Data availability

The data supporting this article have been included as part of the supplementary information (SI). Supplementary information is available. See DOI: https://doi.org/10.1039/d5nj04044b.

CCDC 2472615 contains the supplementary crystallographic data for this paper.[50]

Acknowledgements

References

1 A. W. Czarnik, *Acc. Chem. Res.*, 1994, **27**, 302–308.
2 J. Yi, W. H. Hsieh, J. L. Chir and A. T. Wu, *J. Fluoresc.*, 2014, **24**(6), 1723–1726.
3 L. Chaolong, M. Qin, S. Xu, Y. Yuan, K. Li and J. Tang, *Sens. Actuators, B*, 2024, **407**, 135509.
4 M. Shellaiah, H. C. Chen, K. Awasthi, B. Aazaad, K. W. Sun, N. Ohta and M. C. Lin, *J. Mol. Struct.*, 2024, **1301**, 137347.
5 Y. W. Liu, C. H. Chen and A. T. Wu, *Analyst*, 2012, **137**(22), 5201–5203.
6 S. Muthaiah, B. Aazaad, M. C. Lin, K. W. Sun, A. Murugan, K. Anandan, M. Bhushan, E. Manikandan and W. T. Li, *J. Photochem. Photobiol., A*, 2026, **472**, 116786.
7 K. Kaur, R. Saini, A. Kumar, V. Luxami, N. Kaur, P. Singh and S. Kumar, *Coord. Chem. Rev.*, 2012, **256**, 1992–2028.
8 H. Shinziya, A. K. Das, M. S. Kumar, A. Nag and M. Dolai, *Sens. Diagn.*, 2025, **4**, 622–630.
9 M. S. Kumar, A. K. Das, Y. Bylappa and A. Nag, *RSC Adv.*, 2025, **15**, 6708–6717.
10 S. Vishnu, Y. bylappa, A. Nag, M. Dolai and A. K. Das, *Anal. Methods*, 2024, **16**, 8164–8178.
11 M. S. Kumar and A. K. Das, *New J. Chem.*, 2024, **48**, 13776–13782.
12 A. K. Das and S. Goswami, *Sens. Actuators, B*, 2017, **2045**, 1062–1125.
13 D. Wu, A. C. Sedgwick, T. Gunnlaugsson, E. U. Akkaya, J. Yoon and T. D. James, *Chem. Soc. Rev.*, 2017, **46**, 7105–7123.
14 M. S. Kumar, M. Dolai and A. K. Das, *New J. Chem.*, 2024, **48**, 9103–9109.

15 A. Pundi and C.-J. Chang, *J. Environ. Chem. Eng.*, 2023, **11**, 110346.

16 S. Pakrashy, M. Das, S. Manna, S. M. Choudhury, H. Shinziya, B. Das, M. Dolai and A. K. Das, *Anal. Methods*, 2025, **17**, 6160–6169.

17 S. Vishnu, A. K. Das, G. Karan and S. M. Choudhury, *Mater. Adv.*, 2025, **6**, 4499–4512.

18 S. Vishnu, S. Maity, A. C. Maity, M. S. Kumar, M. Dolai, A. Nag, Y. bylappa, G. Dutta, B. Mukherjee and A. K. Das, *Spectrochim. Acta, Part A*, 2024, **315**, 124249.

19 A. D. Sutton, A. K. Burrell, D. A. Dixon, E. B. Garner 3rd, J. C. Gordon, T. Nakagawa, K. C. Ott, J. P. Robinson and M. Vasiliu, *Science*, 2011, **331**, 1426–1429.

20 S. Huang, X. Qi, T. Liu, K. Wang, W. Zhang, J. Li and Q. Zhang, *Chemistry*, 2016, **22**, 10187–10193.

21 Y.-R. Wang, L. Yang, D.-T. Wang, A.-P. Li, S.-Y. Zhang, L.-L. Qin, Q. Bian, Z.-J. Zhang, Y.-Y. Ding, H. Zhou, D. Peng, G.-H. Wang and Y.-Q. Liu, *Pest Manag. Sci.*, 2025, **81**, 170–184.

22 M. R. Kandler, G. T. Mah, A. M. Tejani, S. N. Stabler and D. M. Salzwedel, *Cochrane Database Syst. Rev.*, 2011, CD004934.

23 D. Poulain, *Crit. Rev. Microbiol.*, 2015, **41**, 208–217.

24 R. Dai, D. J. Wilson, T. W. Geders, C. C. Aldrich and B. C. Finzel, *ChemBioChem*, 2014, **15**, 575–586.

25 K. Ishida, Y. Wada, M. Tachibana, M. Aizawa, M. Fuse, E. Kadoi and H. Takiguchi, *J. Nucl. Sci. Technol.*, 2007, **44**, 222–232.

26 A. Umar, M. M. Rahman, S. H. Kim and Y.-B. Hahn, *Chem. Commun.*, 2008, 166–168.

27 L. Song, D. Gao, S. Li, Y. Wang, H. Liu and Y. Jiang, *J. Chromatogr. B: Anal. Technol. Biomed. Life Sci.*, 2017, **1063**, 189–195.

28 E. Lattová and H. Perreault, *Mass Spectrom. Rev.*, 2013, **32**, 366–385.

29 W. E. Davis 2nd and Y. Li, *Anal. Chem.*, 2008, **80**, 5449–5453.

30 S. Ganesh, F. Khan, M. K. Ahmed and S. K. Pandey, *Talanta*, 2011, **85**, 958–963.

31 J. D. Clark and J. R. Smith, *Anal. Chem.*, 1961, **33**, 1186–1187.

32 R. Tyśkiewicz, M. Fedorowicz, A. Nakonieczna, P. Zielińska, M. Kwiatek and L. Mizak, *Anal. Biochem.*, 2023, **675**, 115215.

33 S. Goswami, A. K. Das, U. Saha, S. Maity, K. Khanra and N. Bhattacharyya, *Org. Biomol. Chem.*, 2015, **13**, 2134–2139.

34 M. Uchiyama, N. Norberto, S. Gonçalves and I. A. Bagatin, *Spectrochim. Acta, Part A*, 2025, **327**, 125356.

35 M. Xing, K. Wang, X. Wu, S. Ma, D. Cao, R. Guan and Z. Liu, *Chem. Commun.*, 2019, **55**, 14980–14983.

36 J. Borah, A. Chetry, A. Pegu, P. Dutta, A. Baruah and P. Khakhlary, *Environ. Sci.: Adv.*, 2025, **7**, 1054–1064.

37 X. Y. Zhang, Y. S. Yang, W. Wang, Q. C. Jiao and H. L. Zhu, *Coord. Chem. Rev.*, 2020, **417**, 213367.

38 K. Semwal and A. K. Das, *RSC Adv.*, 2025, **15**, 10005–10021.

39 Q. Yi, J. He, X. Fu, J. Ying, L. Gong, J. Shen and X. He, *Dyes Pigm.*, 2021, **196**, 109816.

40 N. H. Oza, D. Kasundra, A. G. Deshmukh, N. Borane, R. Boddula and P. N. Patel, *Environ. Sci.: Adv.*, 2025, **4**, 235–244.

41 M. Xing, Y. Han and Y. Zhu, *Anal. Chem.*, 2022, **94**, 12836–12844.

42 S. Singh and J. Kandasamy, *Asian J. Org. Chem.*, 2023, **12**, e202300115.

43 T. Wei, J. Wang, Y. Chen and Y. Han, *RSC Adv.*, 2015, **5**, 57141–57146.

44 A. Samanta, S. Banerjee, T. R. Maity, J. Jahnavi and S. Datta, *Protoplasma*, 2022, **259**, 1455–1466.

45 G. C. Das, A. Kumar Das, D. Das, T. Raj Maity, A. Samanta, F. Ali Alasmary, A. Salem Almalki, A. Iqbal and M. Dolai, *J. Photochem. Photobiol. A Chem.*, 2023, **440**, 114663.

46 S. Baliyan, R. Mukherjee, A. Priyadarshini, A. Vibhuti, A. Gupta, R. P. Pandey and C.-M. Chang, *Molecules*, 2022, **27**, 1326.

47 D. Steinhoff and U. Mohr, *Exp. Pathol.*, 1988, **33**, 133–143.

48 X. Sun, X. Jiang, Z. Wang, Y. Li, J. Ren, K. Zhong, X. Li, L. Tang and J. Li, *J. Hazard Mater*, 2025, **483**, 121442.

49 C. Giacomo, R. Scalenghe and W. I. Woods, *Earth-Sci. Rev.*, 2013, **127**, 1–15.

50 CCDC 2472615: Experimental Crystal Structure Determination, 2025, DOI: 10.5517/ccdc.csd.cc2nzysd.